Supplementary Information

Versatile liquid metal composites constructed by organic-inorganic hybridization strategy for flexible electronics

Xiaoqi Yin, ‡[a] Kangning Sun, ‡[a] Yide Liu,[a] Liwen Tan,[a] Guohong Lin,[a]

Xinpeng Wang,[*,b] Xiankai Li*[*,a]*

[a] College of Materials Science and Engineering, Institute of Marine Biobased Materials, Qingdao University, Ningxia Road 308, Qingdao, 266071, P.R.

[b] Qingdao Central Hospital, School of Rehabilitation Sciences and Engineering, University of Health and Rehabilitation Sciences, Qingdao 266113, China

*To whom correspondence should be addressed: lixk@qdu.edu.cn (X. Li), wangxpd@126.com (X. Wang)

Contents

Supporting Figures

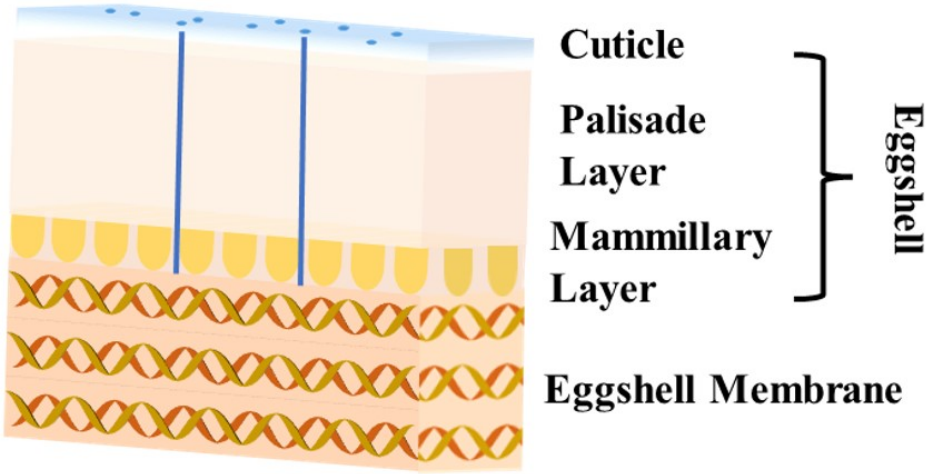

Figure S1. Cross-section of a chicken eggshell, showing its layered composition.

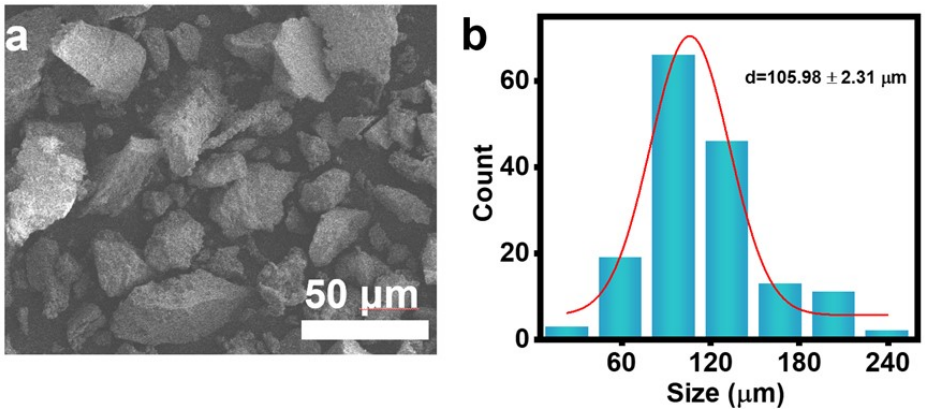

Figure S2. Characterization of eggshell powder. (a) SEM image of eggshell powder. (b) Particle size distribution histogram of eggshell powder.

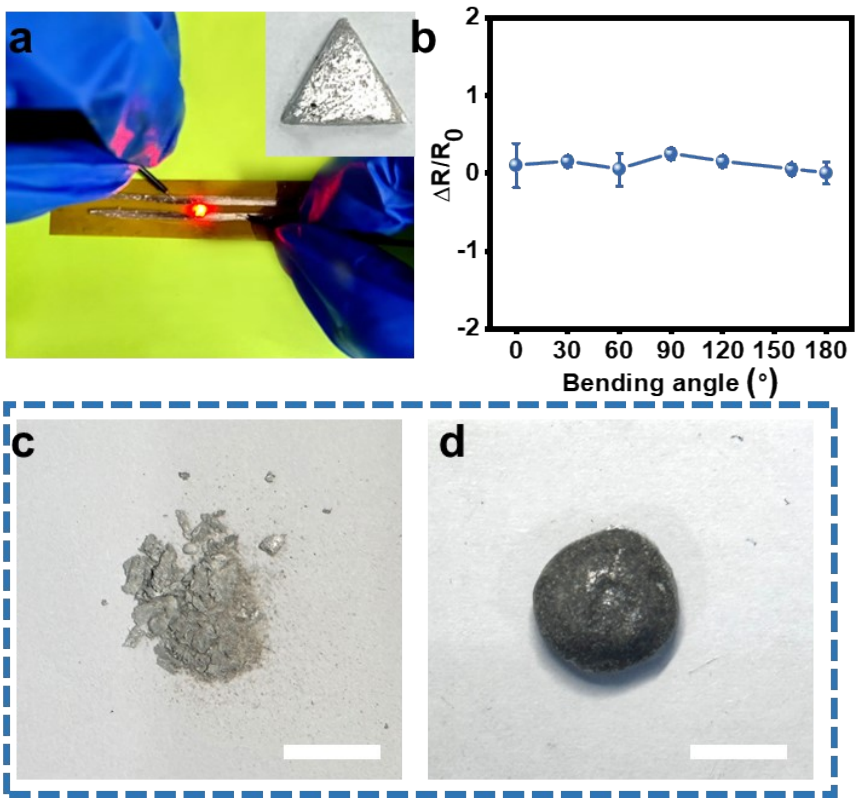

Figure S3. (a) Optical images of the $CaCO_3$-based LM circuit and lighting an LED in flat and bent states. (b) Relative resistance change ($\Delta R/R_0$) under bending angles from 0° to 180° for $CaCO_3$-based LM circuit. (c & d) Optical photographs of the composites prepared via DPM (c) and SAD (d), respectively. Scale bar: 10 mm.

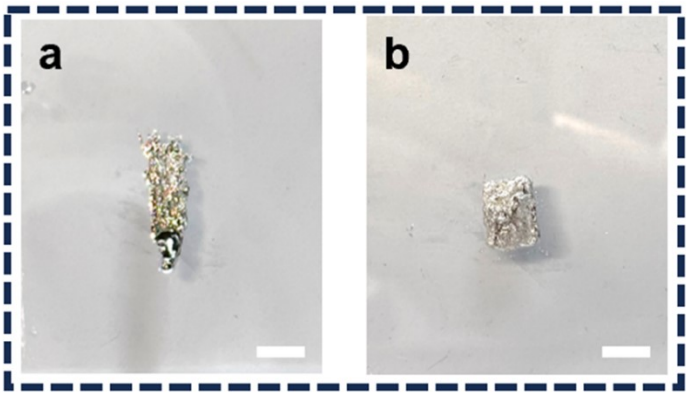

Figure S4. Comparison between liquid metal (LM) and the LM composite. (a) Pure LM and (b) LM composite on tilted glass plates. Scale bar: 10 mm.

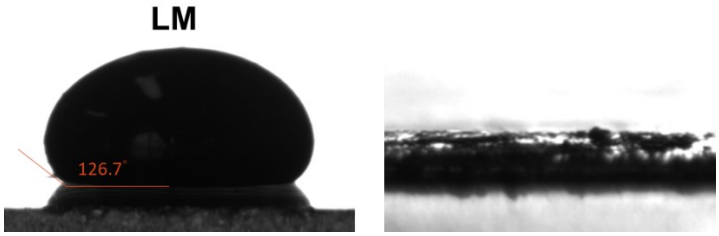

Figure S5. Comparative contact angle measurement of LM and LM composites (with SAD treatment).

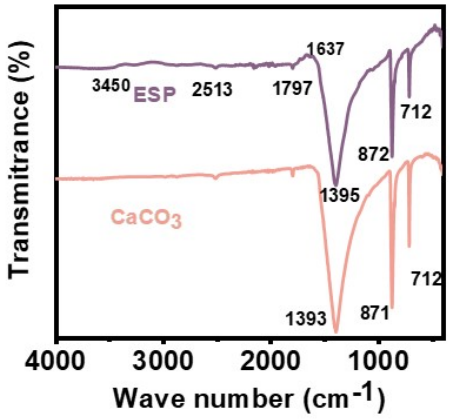

Figure S6. Fourier Transform Infrared Spectroscopy (FTIR) characterization of samples. FTIR spectra of eggshell powder (ESP) and $CaCO_3$.

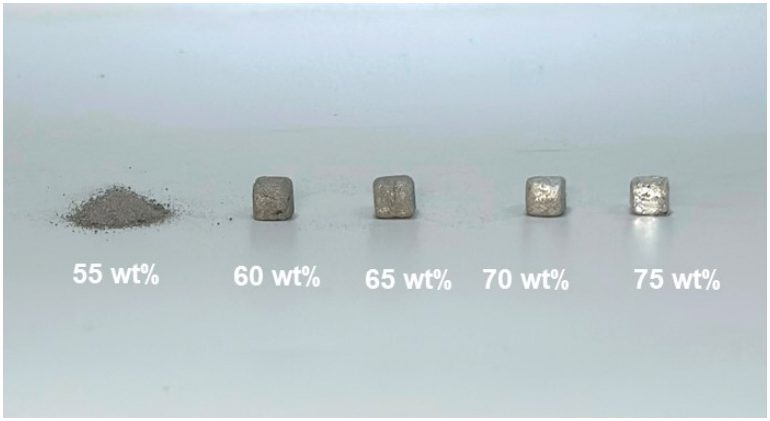

Figure S7. Optical images of sample morphologies at different LM contents (wt%). From left to right, the LM contents are 55 wt%, 60 wt%, 65 wt%, 70 wt%, and 75 wt% in sequence.

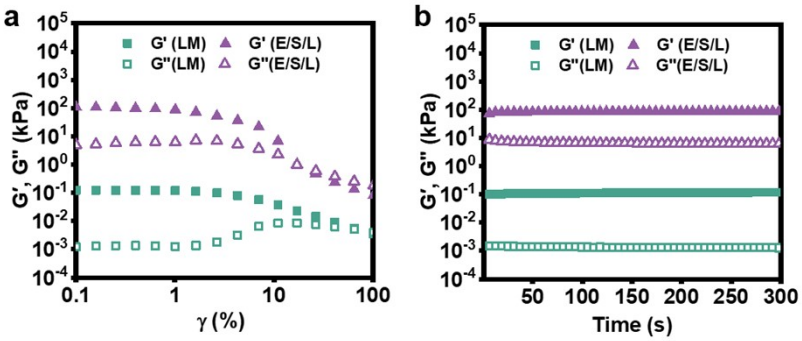

Figure S8. Rheological characterization. (a) Strain amplitude sweep revealing the shear-yielding behavior. (b) Time-sweep measurements displaying temporal stability of the moduli.

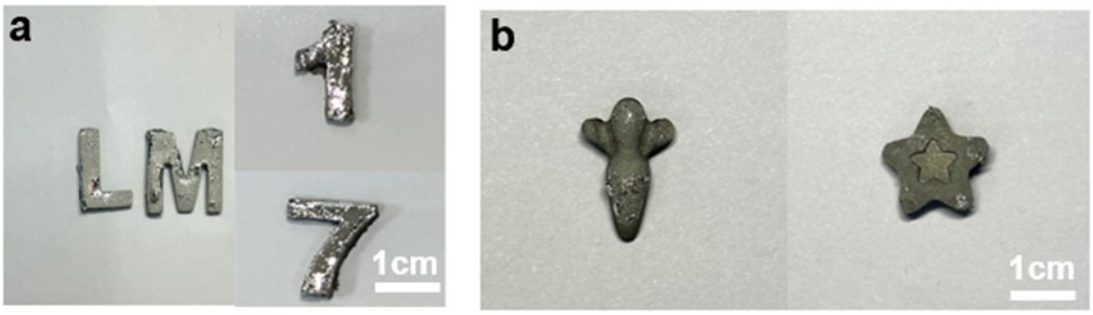

Figure S9. The LM composite exhibits high processability and versatility. It easily reshaped into the letters "LM", numbers "1" and "7", a carrot, and a five-pointed star. Scale bar: 10 mm.

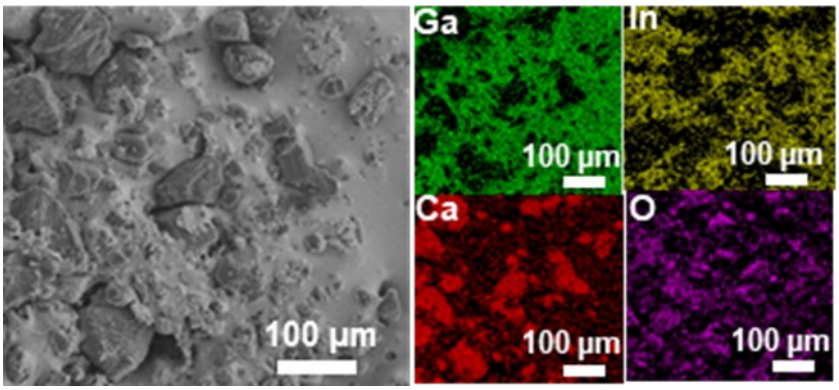

Figure S10. SEM image and EDS elemental mapping of the LM composite with LM of 50 wt%

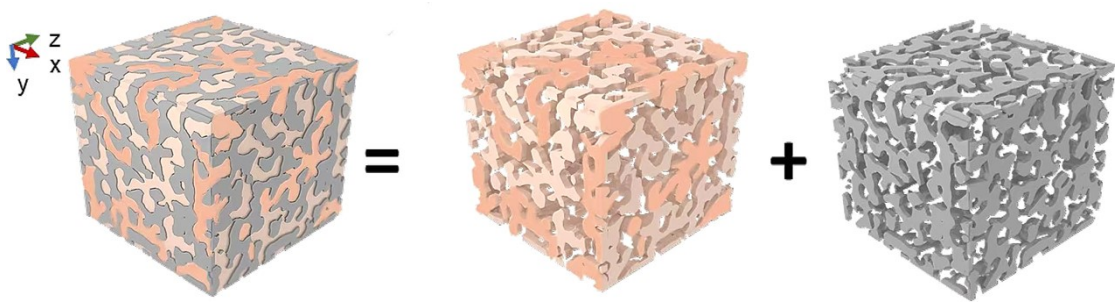

Figure S11. Three-dimensional reconstruction image of the LM composite. Herein, pink represents the organic component, orange represents the inorganic component, and gray represents LM.

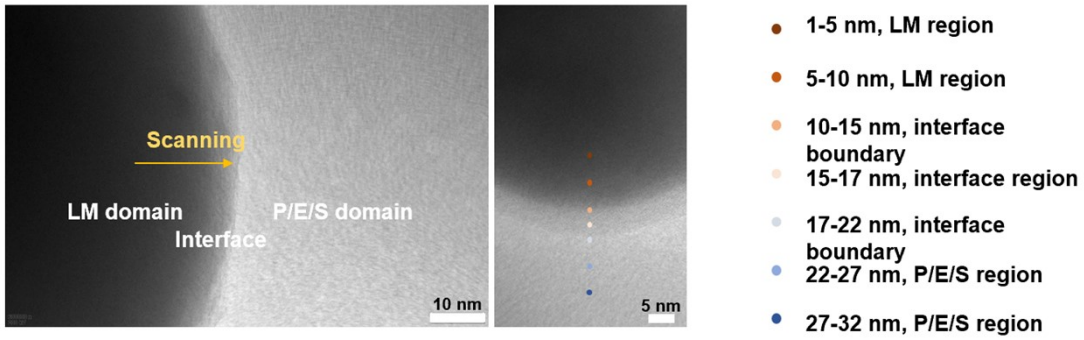

Figure S12. Transmission electron microscopy (TEM) images of the LM composite.

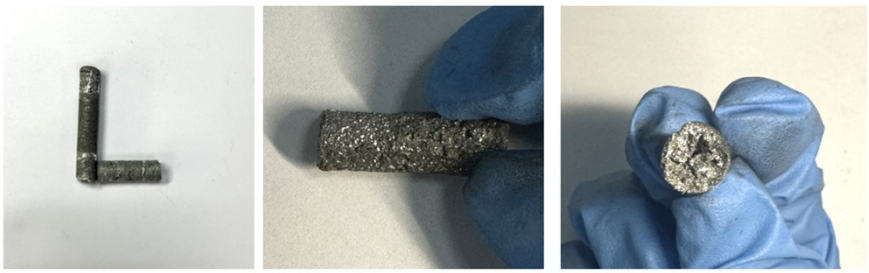

Figure S13. Optical image of liquid metal chalk.

Figure S14. Writing traces of LM chalk on various substrates.

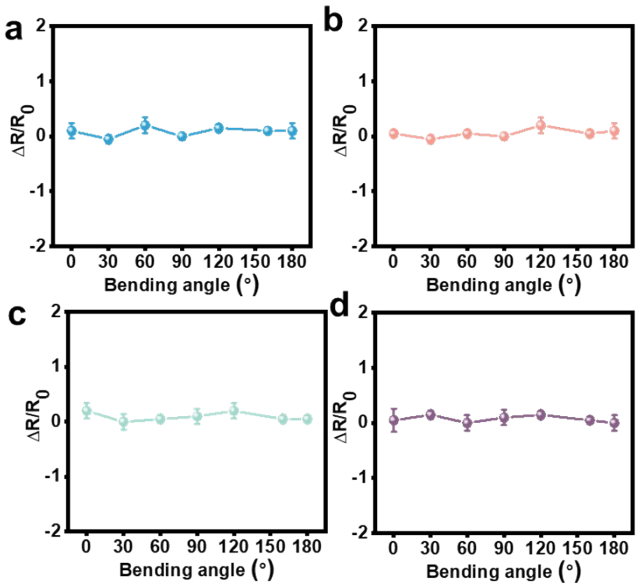

Figure S15. (a)–(d) Relative resistance change ($\Delta R/R_0$) as a function of bending angle for conductive traces on (a) PI, (b) Paper, (c) PE, and (d) glass substrates, respectively.

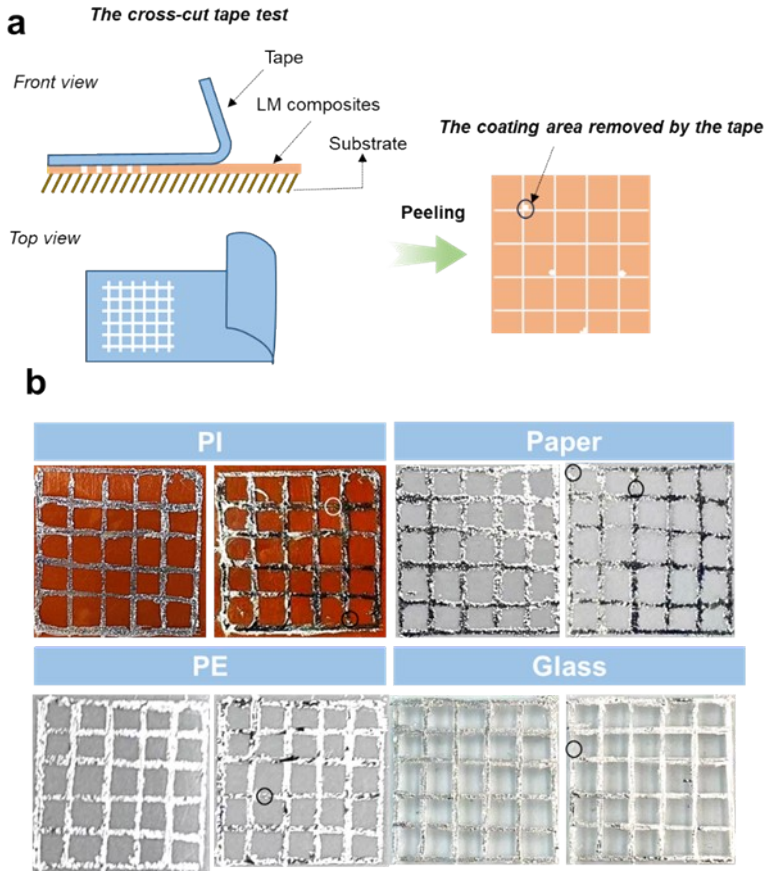

Figure S16. (a) Schematic diagram of the cross-cut tape test; (b) Digital photographs of coatings on different substrates before and after the test.

We characterized the adhesion performance of the LM composite coatings on different substrates via the cross-cut tape test in accordance with the ASTM D3359 standard. The specific test procedure is as follows: first, grid cuts are made on the coating surface, followed by applying and rapidly peeling off the tape. Based on the percentage of coating area removed during tape peeling, the adhesion strength is classified into six grades (5B, 4B, 3B, 2B, 1B, and 0B), corresponding to coating area removal percentages of 0%, 0% – 5%, 5% – 15%, 15% – 35%, 35% – 65%, and greater than 65%, respectively (Fig. S16 (a)). A higher grade (e.g., 5B) indicates stronger adhesion between the coating and the substrate. The test results show that after the cross-cut tape test, the area loss percentage of the direct-written coatings on different substrates is all less than 5%, demonstrating excellent adhesion performance (Grade 4B) between the coatings and the substrates (Fig. S16 (b))

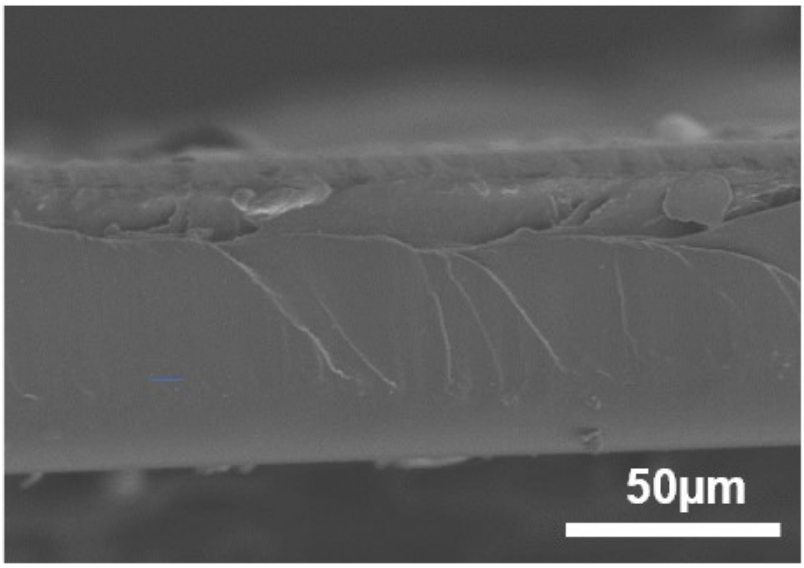

Figure S17. Microscopic characterization of the LM composite prepared by SAD method. SEM image of the cross-section of the composite coating applied to polyimide (PI).

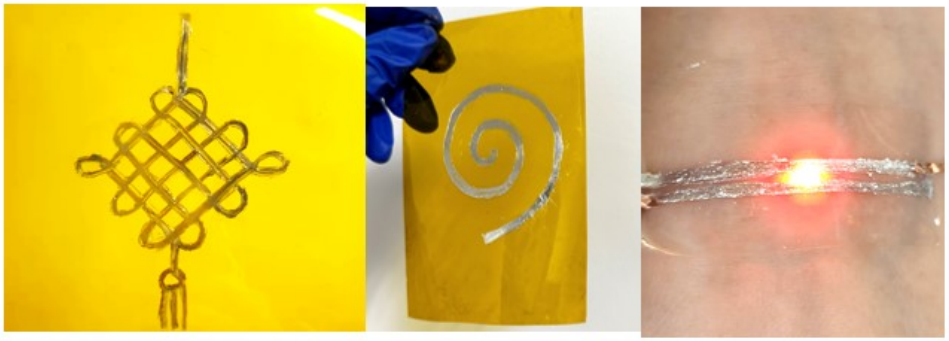

Figure S18. Patterned demonstrations of liquid metal chalk. (left) Chinese knot structure and (middle) spiral pattern, both on PI substrates; (right) flexible circuit on skin powering an LED.

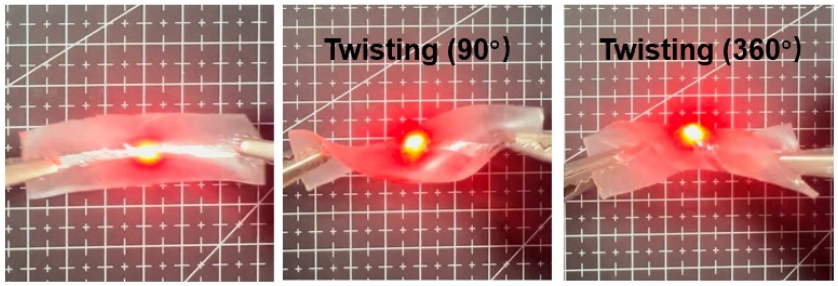

Figure S19. Flexible circuit on styrene-ethylene-butylene-styrene (SEBS) substrate powering an LED under original state (left), 90° twisting (middle), and 360° twisting (right), showing retained conductivity.

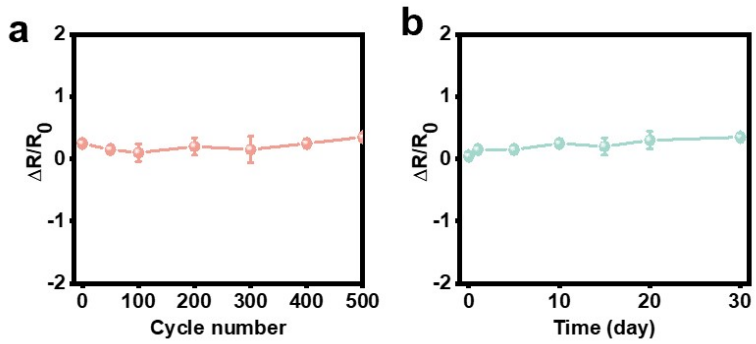

Figure S20. Electrical stability assessment. (a) Resistance variation 500 bending cycles, demonstrating mechanical robustness. (b) Long-term resistance monitoring 30 days, confirming environmental stability against oxidation.

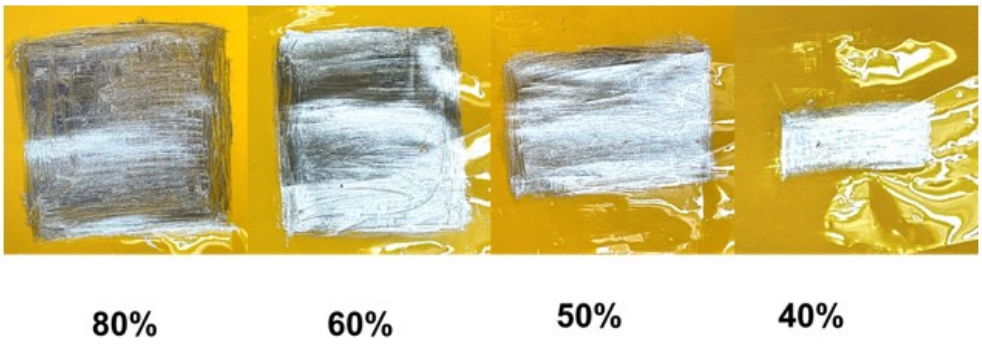

Figure S21. Optical images of coatings on PI substrate fabricated by LM chalks with different LM mass fractions: 80%, 60%, 50%, and 40% (from left to right).

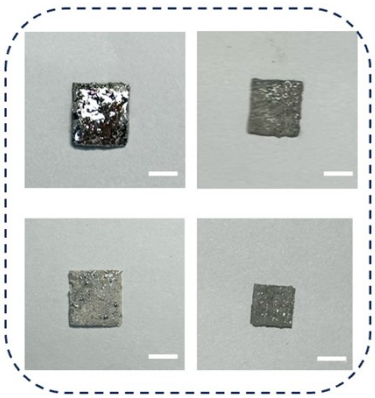

Figure S22. Optical images of LM composite films prepared with different liquid metal contents. Scale bar: 10 mm.

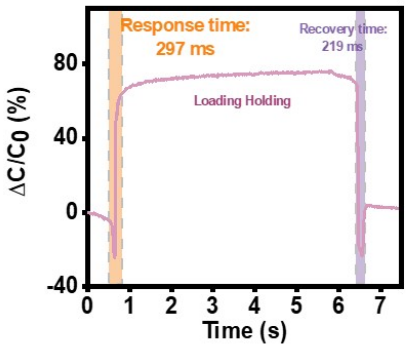

Figure S23. Dynamic response curve of the capacitive sensor fabricated from LM composite. The response time is 297 ms, and the recovery time is 219 ms, with a "Loading Holding" stage shown in the process.

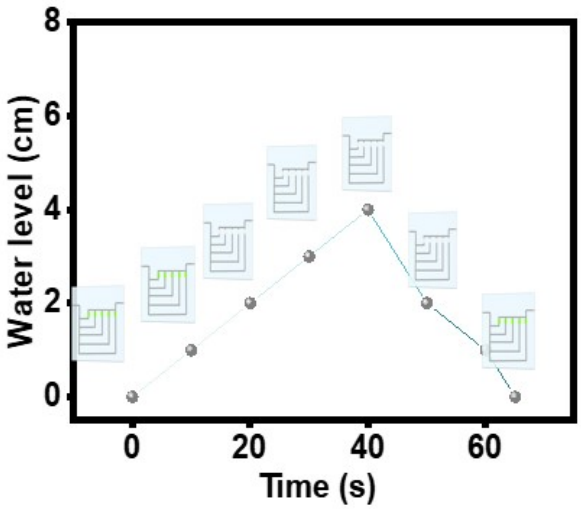

Figure S24. Water level variation curve as a function of time for the water level detection system. Schematic diagrams of the sensor at different time points are inserted to illustrate the corresponding water level states.

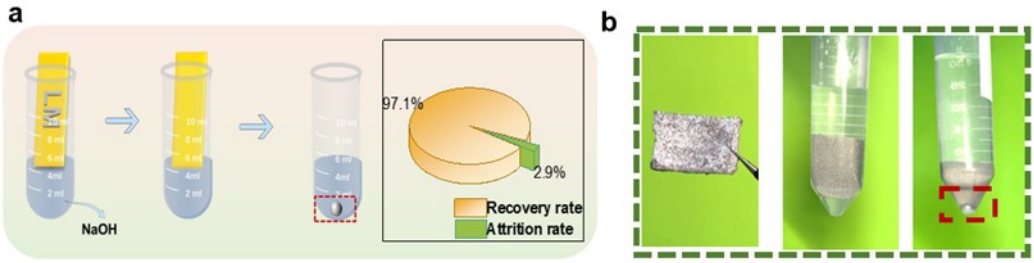

Figure S25. Characterization of LM recovery process. (a) Schematic illustration of LM recovery using NaOH solution, with a pie chart showing recovery rate (97.1%) and attrition rate (2.9%). (b) Optical images of LM material and its dispersion/recovery process in a centrifuge tube.

Table S1. Performance comparison LM based electronics.

	Recyclability	Cost-effectiveness	Recovery rate (%)	Conductivity	Number of substrates	Reference
LM-alcohol/paper	YES	Low	91	NR[b]	1	S1
LM-PVA	YES	Low	96	NR[b]	1	S2
LM-tannic acid/paper	NO	Low	NA[a]	1.6×10^6	10	S3
LM-SiO_2	YES	Low	94	NR[b]	6	S4
LM/graphite	NO	Low	NA[a]	4.9×10^6	6	S5
LM-carbon black)/Exsil 100	NO	Low	NA[a]	5.6	5	S6

LM/poly(3,4-ethylenedioxythiophene	NO	Low	NA[a]	NR[b]	1	[S7]
LM/ESP /Starch/PVA	YES	High	97.1	1.43×10^{6}	10	This work

[a)]NA: not applicable. [b)]NR: not reported;

Table S2. Comparison of various substrates

Substrates	Stability	Adhesion
PI	Good	4B
Paper	Good	4B
PE	Good	4B
Glass	Good	4B

Note S1: Mechanical calculation

According to ASTM standard D790-03, flexural strength (σ_f) and flexural strain (ε_f) of bulk composites are calculated using a three-point bending load-displacement curve with the following equations[S8]:

$$\sigma_f = \frac{3FL}{2BW^2} \quad (1)$$

$$\varepsilon_f = \frac{6Dd}{L^2} \quad (2)$$

where F is the load, L is the span, D is the displacement, and B and W represent the width and thickness of the sample, respectively.

Movie S1. Electrical conductivity stability of liquid metal circuit under stretching.

Movie S2. Color transitions of liquid metal patterns upon turning on the power.

Movie S3. Actuating behavior of liquid metal/sodium alginate film.

Movie S4. The liquid metal/alginate bilayer film can mimic the open-close behavior of flowers.

Movie S5. Recovery of liquid metal in NaOH solution.

Supporting References[1–7]

(S1) F. Li, Q. Qin, Y. Zhou, Y. Wu, W. Xue, S. Gao, J. Shang, Y. Liu and R. Li, *Adv. Mater. Technol.*, 2018, **3**, 1800131.

(S2) L. Teng, S. Ye, S. Handschuh-Wang, X. Zhou, T. Gan and X. Zhou, *Adv. Funct. Mater*., 2019, **29**, 1808739.

(S3) Md. A. Rahim, F. Centurion, J. Han, R. Abbasi, M. Mayyas, J. Sun, M. J. Christoe, D. Esrafilzadeh, F. Allioux, M. B. Ghasemian, J. Yang, J. Tang, T. Daeneke, S. Mettu, J. Zhang, M. H. Uddin, R. Jalili and K. Kalantar-Zadeh, *Adv. Funct. Mater.*, 2021, **31**, 2007336.

(S4) H. Chang, P. Zhang, R. Guo, Y. Cui, Y. Hou, Z. Sun and W. Rao, *ACS Appl. Mater. Interfaces*, 2020, **12**, 14125–14135.

(S5) Q. Li, W. Peng, Y. Sun, C. Cai, F. Tang, Y. Liu, Q. Hu, Z. Zhou, X. Li and S. Nie, *Bioresour. Technol.*, 2024, **402**, 130802.

(S6) M. Singh, P. Bhuyan, S. Jeong and S. Park, *Adv. Funct. Mater.*, 2024, 2412178.

(S7) J.-E. Park, H. S. Kang, J. Baek, T. H. Park, S. Oh, H. Lee, M. Koo and C. Park, *ACS Nano*, 2019, **13**, 9122–9130.

(S8) J. Yan, T. Zhou, J. Peng, H. Wang, L. Jiang and Q. Cheng, *Sci. Bull.*, 2024, **69**, 913–921.